

Analysis of the September ϵ -Perseid outburst in 2013

José M. Madiedo,^{1*} Jaime Zamorano,² Josep M. Trigo-Rodríguez,^{3,4} José L. Ortiz,⁵
 José A. Docobo,⁶ Jaime Izquierdo,² Juan Lacruz,⁷ Pedro P. Campo,⁶
 Manuel Andrade,^{8,6} Sensi Pastor,⁹ José A. de los Reyes,⁹ Francisco Ocaña,^{2,10}
 Alejandro Sánchez-de Miguel^{2,11} and Pep Pujols¹²

¹Facultad de Ciencias Experimentales, Universidad de Huelva, E-21071 Huelva, Spain

²Dpto. de Física de la Tierra y Astrofísica, Facultad de Ciencias Físicas, Universidad Complutense de Madrid, E-28040 Madrid, Spain

³Institute of Space Sciences (CSIC), Campus UAB, Facultat de Ciències, Torre C5-parell-2^a, E-08193 Bellaterra, Barcelona, Spain

⁴Institut d'Estudis Espacials de Catalunya (IEEC), Edif. Nexus, c/Gran Capità, 2–4, E-08034 Barcelona, Spain

⁵Instituto de Astrofísica de Andalucía, CSIC, Apt. 3004, Camino Bajo de Huétor 50, E-18080 Granada, Spain

⁶Observatorio Astronómico Ramón María Aller (OARMA). Universidade de Santiago de Compostela, Avenida das Ciencias, Campus Vida. E-15782 Santiago de Compostela, Spain

⁷La Cañada Observatory (MPC J87), E-05003 Ávila, Spain

⁸Departamento de Matemática Aplicada. Escola Politécnica Superior de Enxeñaría, Universidade de Santiago de Compostela, Campus Universitario, E-27002 Lugo, Spain

⁹Observatorio Astronómico de La Murta. Molina de Segura, E-30500 Murcia, Spain

¹⁰Quasar Science Resources, S. L., Las Rozas de Madrid, E-28232 Madrid, Spain

¹¹Environment and Sustainability Institute, University of Exeter, Penryn, Cornwall TR10 9FE, UK

¹²Agrupació Astronòmica d'Osona (AAO), Carrer Pare Xifré 3, 3er. 1a., E-08500 Vic, Barcelona, Spain

Accepted 2018 July 16. Received 2018 June 24; in original form 2018 April 24

ABSTRACT

We analyse the outburst experienced by the September ϵ -Perseid meteor shower on 2013 September 9. As a result of our monitoring, the atmospheric trajectory of 60 multistation events observed over Spain was obtained and accurate orbital data were derived from them. On the basis of these orbits, we have tried to determine the likely parent body of this meteoroid stream by employing orbital dissimilarity criteria. In addition, the emission spectra produced by two events belonging to this meteor shower were also recorded. The analysis of these spectra has provided information about the chemical nature of their progenitor meteoroids. We also present an estimation of the tensile strength for these particles.

Key words: meteorites, meteors, meteoroids.

1 INTRODUCTION

The September ϵ -Perseid (SPE) meteoroid stream gives rise to an annual display of meteors from about September 7 to 23, peaking around September 12 (Jenniskens 2006). This minor shower was first observed by Denning (1882), and is currently included in the IAU list of meteor showers with code 208 SPE. No systematic analysis of this shower was performed during the early-to-mid 20th century, and the first reliable data about this stream were analysed in Hoffmeister (1948). The next observations were published by Trigo-Rodríguez (1989), who clearly identified SPE activity over the sporadic background, with often trained and bright meteors exhibiting a peak zenithal hourly rate ZHR = 5 meteors h⁻¹ in 1989.

Only two outbursts of SPE meteor activity have been reported. The first of these was unexpected and took place on 2008 September 9, with an activity consisting mostly of bright meteors (Jenniskens et al. 2008; Rendtel and Molau 2010). This outburst was not favourable for observers in Europe. So, despite our systems were monitoring the night sky, we could not record this activity increase. The second SPE outburst occurred on 2013 September 9. It took place between 21 h 30 m and 23 h 20 m UT and was confirmed in Jenniskens (2013). On the basis of the results obtained from the analysis of the 2008 outburst, and by assuming that SPE meteoroids were produced by a long-period comet that ejected these particles before the year 1800 AD, Jenniskens (2013) inferred that this dust trail should encounter Earth on 2013 September 9 at 22 h 15 m UT. This is in good agreement with the circumstances of the 2013 SPE outburst. However, the parent comet of this stream has not been identified yet. Accurate orbital data obtained from the analysis of SPE meteors could help to find the likely parent of the SPEs. And meteor spectroscopy can also play an important role to derive

* E-mail: madiedo@cica.es

information about the chemical nature of these meteoroids and their progenitor body.

Optimal weather conditions over most of the Iberian Peninsula during the first half of 2013 September allowed us to analyse the meteor activity produced by the SPE stream. In this work, we focus on the analysis of the 2013 SPE outburst. From our recordings, we have obtained orbital information about meteoroids belonging to this poorly known stream. The tensile strength of these particles is also estimated. Besides, two emission spectra produced by SPE meteors are also analysed. These are, to our knowledge, the first SPE spectra discussed in the scientific literature.

2 INSTRUMENTATION AND DATA REDUCTION TECHNIQUES

The meteor observing stations that were involved in the monitoring of the SPE outburst analysed here are listed in Table 1. These employ between 3 and 12 high-sensitivity CCD video cameras (models 902H and 902H Ultimate from Watec Co., Japan) to monitor the night sky (Madiedo & Trigo-Rodríguez 2008; Trigo-Rodríguez et al. 2009, Madiedo et al. 2010). Their field of view ranges from 90×72 to 14×11 deg. These CCD devices work according to the PAL video standard and, so, they generate interlaced video imagery at 25 fps with a resolution of 720×576 pixels. More details about these devices and the way they are operated are given, for instance, in (Madiedo 2014). In order to obtain the atmospheric trajectory of the meteors and the heliocentric orbit of the progenitor meteoroids, we have employed the AMALTHEA software (Madiedo et al. 2013a,b), which follows the methods described in Ceplecha (1987).

To record meteor emission, we have attached holographic diffraction gratings (with 500 or 1000 lines/mm, depending on the device) to the objective lens of some of the above-mentioned CCD video cameras. With these slitless videospectrographs, we can record the emission spectrum of meteors brighter than magnitude $-3/-4$ (Madiedo et al. 2013c; Madiedo 2014). The analysis of the emission spectra obtained during the SPE observing campaign analysed here was performed by means of the CHIMET software (Madiedo et al. 2013c).

3 OBSERVATIONS AND RESULTS

In 2013, our meteor observing stations observed activity from the SPEs from September 1 to 12. On 2013 September 9, at about 21 h 35 m UT, our CCD video devices registered a marked increase in meteor activity associated with this stream, including some fireballs. A careful checking of these data confirmed the SPE outburst between around 21 h 35 m UT on September 9 and 0 h 20 m UT on September 10, in good agreement with the circumstances described in Jenniskens (2013). From the analysis of the multistation events recorded from sites listed in Table 1, we have obtained the atmospheric trajectory of these meteors. However, we just took into consideration those trails for which the convergence angle was above 20 deg. This parameter, which is usually employed to measure the quality of the results, is the angle between the two planes delimited by the observing sites and the meteor atmospheric path (Ceplecha 1987). A total of 60 SPE meteors satisfied this condition. These events are listed in Table 2, which shows the absolute peak magnitude (M), the initial (pre-atmospheric) photometric mass of the progenitor meteoroid (m_p), the initial (H_b) and final (H_e) heights of the meteor, the right ascension (α_g) and declination (δ_g) of the geocentric radiant (J2000.0), and the pre-atmospheric (V_∞) and geocentric (V_g) velocities. To identify each meteor, we have employed

a code with the format DDYYEE, where DD is the day of the month (which ranges between 01 and 12 for the meteors analysed here), and YY corresponds to the last two digits of the recording year. The two digit EE is employed to number meteors recorded during the same night, so that 00 is assigned to the first meteor imaged, 01 to the second one, and so on. The averaged value for the observed initial (pre-atmospheric) velocity was $V_\infty = 65.9 \pm 0.2$ km s⁻¹. The photometric mass of the parent meteoroids ranged between 0.01 and 16 g (Table 2). The orbital parameters derived for the meteoroids that gave rise to these meteor events are listed in Table 3.

4 DISCUSSION

4.1 Parent body

The averaged orbital data calculated by taking into account a total of $N = 60$ SPE orbits are shown in Table 3. This table also includes the average orbit of meteors observed during the outburst ($N = 28$ meteors). As can be noticed, the difference between both averaged orbits is not significant. With these parameters, we have obtained that the value of the Tisserand parameter with respect to Jupiter yields $T_J = -0.65 \pm 0.44$. This agrees with the assumption in Jenniskens (2013) that SPE meteoroids are produced by a long-period comet.

Besides, we have calculated the so-called K_B parameter, which according to Ceplecha (1988) can be employed to classify meteoroids into four different populations: A-group, comprising particles similar to carbonaceous chondrites ($7.3 \leq K_B < 8$); B-group of dense cometary material ($7.1 \leq K_B < 7.3$); C-group of regular cometary material ($6.6 \leq K_B < 7.1$); and D-group of soft cometary material ($K_B < 6.6$). This parameter is defined by the following equation:

$$K_B = \log \rho_B + 2.5 \log V_\infty - 0.5 \log \cos z_R + 0.15, \quad (1)$$

where ρ_B is the air density at the beginning of the luminous trajectory (in g cm⁻³), V_∞ is the pre-atmospheric velocity of the meteoroid (in cm s⁻¹), and z_R is the inclination of the atmospheric trajectory with respect to the vertical. We have obtained the air density ρ_B by using the NRLMSISE-00 atmosphere model (Picone et al. 2002). According to our computations, the average K_B parameter for the SPE events in Table 2 yields $K_B = 6.9 \pm 0.2$. This result suggests that meteoroids in this stream belong to the group of regular cometary materials.

We have tried to determine the likely parent comet of SPE meteoroids by means of orbital dissimilarity criteria (Williams 2011). In this approach, we have employed the ORAS program (ORbital Association Software) to search through the Minor Planet Center data base in order to establish a potential link between the SPE stream and other bodies in the Solar system (Madiedo et al. 2013d). This analysis has been performed by calculating the Southworth and Hawkins D_{SH} criterion (Southworth & Hawkins 1963). However, the lowest values obtained for the D_{SH} function are of about 1.50, which is well above the $D_{SH} < 0.15$ cut-off value usually adopted to validate a potential association (Lindblad 1971a,b). So we conclude that the parent comet of the SPE stream is not catalogued.

4.2 Meteor initial and final heights

The dependence with meteoroid mass of the beginning and final heights of meteors analysed in this work has been plotted in Figs 1 and 2, respectively. As can be seen in Fig. 1, the initial height H_b increases with increasing meteoroid mass. This behaviour has been

Table 1. Geographical coordinates of the SPMN meteor observing stations that recorded the 2013 outburst of the SPE meteor shower.

Station #	Station name	Longitude	Latitude (N)	Altitude (m)
1	Sevilla	5° 58' 50" W	37° 20' 46"	28
2	La Hita	3° 11' 00" W	39° 34' 06"	674
3	Huelva	6° 56' 11" W	37° 15' 10"	25
4	Sierra Nevada	3° 23' 05" W	37° 03' 51"	2896
5	El Arenosillo	6° 43' 58" W	37° 06' 16"	40
6	Cerro Negro	6° 19' 35" W	37° 40' 19"	470
7	Ávila	4° 29' 30" W	40° 36' 18"	1400
8	Villaverde del Ducado	2° 29' 29" W	41° 00' 04"	1100
9	Madrid-UCM	3° 43' 34" W	40° 27' 03"	640
10	La Murta	1° 12' 10" W	37° 50' 25"	400
11	Folgueroles	2° 19' 33" E	41° 56' 31"	580
12	Montseny	2° 32' 01" E	41° 43' 47"	194
13	Lugo	7° 32' 41" W	42° 59' 35"	418
14	OARMA	8° 33' 34" W	42° 52' 31"	240

also found for other meteor showers with a cometary origin (see e.g. Jenniskens 2004; Kotten et al. 2004; Madiedo 2015). We have described this behaviour by means of a linear relationship between H_b and the logarithm of the meteoroid photometric mass (solid line in Fig. 1). The slope of this line is 2.38 ± 0.70 . According to this result, the increase of the beginning height with meteoroid mass is less important for the SPEs than for the Leonids ($a = 9.9 \pm 1.5$), the Perseids ($a = 7.9 \pm 1.3$), the Taurids ($a = 6.6 \pm 2.2$), and the Orionids ($a = 5.02 \pm 0.65$) (Kotten et al. 2004). But more pronounced than for the ρ -Geminids ($a = 1.1 \pm 0.5$), which are produced by tough cometary meteoroids (Madiedo 2015), and the Geminids ($a = 0.46 \pm 0.26$) (Kotten et al. 2004), which have an asteroidal origin (Jenniskens 2004). Despite the pre-atmospheric velocity of the SPEs and the Perseids is similar (~ 65 and ~ 61 km s^{-1} , respectively), the beginning height exhibited by SPE meteors is significantly lower. Thus, for instance, for SPE meteors H_b is below 110 km for a meteoroid mass of about 0.02 g (Fig. 2), but ~ 120 km for Perseid members with the same mass (Kotten et al. 2004). This suggests that SPE meteoroids are tougher.

The larger is the meteoroid mass, the lower is the terminal point H_e of the meteor (Fig. 2). The slope of the line we have employed to model this behaviour (solid line in Fig. 2) yields -2.25 ± 0.45 . Since slower meteoroids tend to penetrate deeper in the atmosphere, it is not surprising that SPE meteoroids, which exhibit an initial velocity of ~ 65 km s^{-1} , do not penetrate as deep as the Perseids with a pre-atmospheric velocity of ~ 61 km s^{-1} (Kotten et al. 2004), the Geminids with a velocity of ~ 36 km s^{-1} (Jenniskens 2004), or the ρ -Geminids with a velocity of about 23 km s^{-1} (Madiedo 2015).

4.3 Meteoroid strength

The tensile strength of meteoroids ablating in the atmosphere can be estimated by analysing the flares exhibited by the corresponding meteors. According to this approach, these flares take place as a consequence of the sudden break-up of the meteoroid when the aerodynamic pressure overcomes the strength of the particle (Trigo-Rodríguez & Llorca 2006). However, SPE events listed in Table 2 exhibited a quasi-continuous ablation behaviour, with smooth light curves that revealed that no flares occurred during their interaction with the atmosphere. So, we have employed this technique to evaluate the maximum aerodynamic pressure suffered by SPE meteoroids, which has provided a lower limit for their tensile strength. This aerodynamic pressure S can be estimated by using the follow-

ing relationship (Bronshen 1981):

$$S = \rho_{\text{atm}} \cdot v^2, \quad (2)$$

where ρ_{atm} and v are the atmospheric density and meteor velocity at a given height, respectively. In this work, we have calculated the air density by employing the NRLMSISE-00 atmosphere model (Picone et al. 2002). From the analysis of the atmospheric trajectory calculated for meteors in Table 2, we have obtained a maximum aerodynamic pressure of $(2.9 \pm 0.3) \cdot 10^5$ dyn cm^{-2} . This value is higher than the average strength found for Quadrantid and Perseid meteoroids [$\sim 2 \cdot 10^5$ and $(1.2 \pm 0.3) \cdot 10^5$ dyn cm^{-2} , respectively], and below the strength of the Taurids [$(3.4 \pm 0.7) \cdot 10^5$ dyn cm^{-2}] (Trigo-Rodríguez & Llorca 2006, 2007).

4.4 Emission spectra

The video spectrographs operated at stations 1–6 in Table 1 recorded a total of eight SPE emission spectra during the outburst recorded on September 9–10. Unfortunately, six of these were too dim to be analysed, but the other two had enough quality to provide information about the chemical nature of these meteoroids. These spectra were produced by meteors labelled as SPE091327 and SPE091331 in Table 2, respectively. They have been analysed with the CHIMET software (Madiedo et al. 2013c), which first deinterlaces the video files containing these signals. Then, the software performs a dark-frame subtraction, and each video frame is flat-fielded. Next, the calibration in wavelength is achieved by identifying emission lines typically found in meteor spectra. Then, the intensity of the signals is corrected by taking into account the spectral efficiency of the spectrograph. The results obtained from this procedure are shown in Figs 3 and 4. In these plots, the most remarkable multiplets have been labelled according to the notation given by Moore (1945). The most noticeable emissions correspond to the atmospheric O I line at 777.4 nm, and to the K and H lines of Ca II-1 at 393.3 and 396.8 nm, respectively. These two lines produced by ionized calcium appear blended in the spectrum. Other prominent contributions are those of Fe I-41 (440.4 nm), the Mg I-2 triplet (517.3 nm), and the Na I-1 doublet (588.9 nm). The emission of atmospheric N_2 bands was also identified in the red region of the spectrum.

As in previous works (see e.g. Madiedo et al. 2014), we have investigated the chemical nature of the progenitor meteoroids by analysing the relative intensity of the Na I-1, Mg I-2, and Fe I-15 multiplets in these spectra (Borovička et al. 2005). To perform this analysis, the intensity (in arbitrary units) of the emission lines

Table 2. Trajectory and radiant data (J2000) for the double-station SPE meteors discussed in the text.

Meteor code	Date	Time (UT) ± 0.1 s	$M \pm 0.5$	m_p (g)	H_b (km) ± 0.5	H_e (km) ± 0.5	α_g ($^\circ$)	δ_g ($^\circ$)	V_∞ (km s $^{-1}$)	V_g (km s $^{-1}$)
01 1301	Sep 1	4h16m25.8s	-2.0	0.17 \pm 0.07	109.4	88.0	41.31 \pm 0.10	38.15 \pm 0.02	66.2 \pm 0.2	65.2 \pm 0.2
01 1302	Sep 1	20h50m52.3s	1.2	0.01 \pm 0.01	109.5	100.6	42.45 \pm 0.07	37.04 \pm 0.02	66.9 \pm 0.2	65.7 \pm 0.2
01 1303	Sep 1	23h22m20.4s	-2.1	0.19 \pm 0.08	116.6	99.5	41.88 \pm 0.08	37.45 \pm 0.02	66.6 \pm 0.2	65.4 \pm 0.2
02 1301	Sep 2	1h15m45.0s	-0.5	0.04 \pm 0.01	111.2	90.5	42.03 \pm 0.10	38.14 \pm 0.04	66.5 \pm 0.2	65.3 \pm 0.2
02 1302	Sep 2	2h44m43.2s	-1.2	0.08 \pm 0.03	112.1	95.6	42.08 \pm 0.09	37.72 \pm 0.06	66.2 \pm 0.2	65.1 \pm 0.2
03 1301	Sep 3	1h25m30.3s	-2.7	0.35 \pm 0.14	113.3	92.0	41.58 \pm 0.12	36.55 \pm 0.10	66.3 \pm 0.2	65.1 \pm 0.2
03 1302	Sep 3	3h53m12.9s	-0.7	0.05 \pm 0.02	109.9	91.4	42.13 \pm 0.15	37.86 \pm 0.09	66.0 \pm 0.2	65.0 \pm 0.2
04 1301	Sep 4	1h04m43.8s	0.5	0.01 \pm 0.01	109.5	98.8	43.11 \pm 0.14	36.74 \pm 0.10	66.4 \pm 0.2	65.2 \pm 0.2
05 1301	Sep 5	1h17m19.2s	-2.5	0.29 \pm 0.12	113.9	87.6	44.09 \pm 0.15	37.62 \pm 0.10	66.5 \pm 0.2	65.3 \pm 0.2
05 1302	Sep 5	21h11m18.1s	-3.6	0.86 \pm 0.35	115.6	101.8	44.24 \pm 0.14	38.23 \pm 0.10	66.1 \pm 0.2	64.8 \pm 0.2
06 1301	Sep 6	4h59m48.6s	-3.9	1.16 \pm 0.47	114.1	90.1	44.48 \pm 0.10	38.10 \pm 0.10	65.8 \pm 0.2	64.9 \pm 0.2
08 1301	Sep 8	2h21m15.4s	1.1	0.01 \pm 0.01	107.6	96.9	45.39 \pm 0.07	38.72 \pm 0.08	65.7 \pm 0.2	64.6 \pm 0.2
08 1302	Sep 8	3h29m08.9s	-3.6	0.86 \pm 0.35	110.4	89.8	46.47 \pm 0.12	38.40 \pm 0.09	65.9 \pm 0.2	64.9 \pm 0.2
08 1303	Sep 8	4h00m40.7s	-3.4	0.71 \pm 0.29	115.4	84.4	45.97 \pm 0.15	38.26 \pm 0.12	65.8 \pm 0.2	64.8 \pm 0.2
09 1301	Sep 9	0h13m42.3s	0.8	0.01 \pm 0.01	105.5	89.0	47.28 \pm 0.09	38.99 \pm 0.10	66.1 \pm 0.2	64.9 \pm 0.2
09 1302	Sep 9	0h52m35.4s	1.0	0.01 \pm 0.01	111.0	95.4	47.16 \pm 0.09	39.01 \pm 0.08	66.0 \pm 0.2	64.8 \pm 0.2
09 1303	Sep 9	1h31m29.7s	-2.1	0.20 \pm 0.08	113.3	97.6	47.20 \pm 0.10	38.94 \pm 0.09	66.1 \pm 0.2	65.0 \pm 0.2
09 1304	Sep 9	1h37m55.5s	1.5	0.01 \pm 0.01	101.1	96.8	47.12 \pm 0.08	39.00 \pm 0.08	65.9 \pm 0.2	64.7 \pm 0.2
09 1305	Sep 9	2h34m02.9s	-0.9	0.06 \pm 0.02	109.9	95.4	47.54 \pm 0.10	38.92 \pm 0.09	66.0 \pm 0.2	64.9 \pm 0.2
09 1306	Sep 9	21h43m34.0s	-1.2	0.08 \pm 0.03	107.6	97.2	47.78 \pm 0.09	39.28 \pm 0.09	66.0 \pm 0.2	64.8 \pm 0.2
09 1307	Sep 9	21h53m24.2s	-5.1	3.87 \pm 1.57	116.1	94.8	47.76 \pm 0.10	39.53 \pm 0.10	65.9 \pm 0.2	64.6 \pm 0.2
09 1308	Sep 9	21h56m32.7s	-1.9	0.16 \pm 0.06	116.6	105.0	47.84 \pm 0.10	39.17 \pm 0.09	66.1 \pm 0.2	64.8 \pm 0.2
09 1309	Sep 9	21h56m51.3s	-3.4	0.72 \pm 0.29	114.3	85.1	47.92 \pm 0.08	39.76 \pm 0.06	65.9 \pm 0.2	64.7 \pm 0.2
09 1310	Sep 9	21h58m13.5s	0.1	0.01 \pm 0.01	101.7	97.1	47.72 \pm 0.09	39.75 \pm 0.09	65.9 \pm 0.2	64.6 \pm 0.2
09 1311	Sep 9	22h00m44.5s	0.3	0.02 \pm 0.01	101.5	96.9	47.51 \pm 0.09	39.67 \pm 0.08	65.8 \pm 0.2	64.5 \pm 0.2
09 1312	Sep 9	22h00m56.1s	-2.8	0.39 \pm 0.15	115.2	88.1	47.41 \pm 0.09	39.57 \pm 0.08	65.8 \pm 0.2	64.6 \pm 0.2
09 1313	Sep 9	22h01m17.6s	-5.7	7.5 \pm 3.0	118.2	87.3	47.32 \pm 0.08	39.37 \pm 0.08	65.7 \pm 0.2	64.4 \pm 0.2
09 1314	Sep 9	22h02m23.9s	-0.5	0.03 \pm 0.01	105.1	95.9	47.51 \pm 0.08	39.76 \pm 0.08	65.8 \pm 0.2	64.5 \pm 0.2
09 1315	Sep 9	22h04m01.2s	-2.2	0.20 \pm 0.08	112.9	97.2	47.60 \pm 0.09	39.67 \pm 0.08	65.9 \pm 0.2	64.6 \pm 0.2
09 1316	Sep 9	22h04m20.3s	-5.2	4.58 \pm 1.86	116.7	95.2	47.90 \pm 0.09	39.71 \pm 0.09	66.0 \pm 0.2	64.7 \pm 0.2
09 1317	Sep 9	22h04m46.8s	1.5	0.01 \pm 0.01	100.5	96.3	47.80 \pm 0.10	39.82 \pm 0.07	65.9 \pm 0.2	64.6 \pm 0.2
09 1318	Sep 9	22h05m04.0s	-0.6	0.04 \pm 0.02	115.6	107.1	47.81 \pm 0.09	39.47 \pm 0.08	65.9 \pm 0.2	64.6 \pm 0.2
09 1319	Sep 9	22h08m10.7s	-3.0	0.48 \pm 0.20	111.9	95.1	47.40 \pm 0.11	39.78 \pm 0.07	65.7 \pm 0.2	64.5 \pm 0.2
09 1320	Sep 9	22h09m57.0s	-1.8	0.14 \pm 0.05	113.0	97.0	47.88 \pm 0.10	39.48 \pm 0.08	65.9 \pm 0.2	64.6 \pm 0.2
09 1321	Sep 9	22h13m24.3s	-4.6	2.5 \pm 1.0	115.2	86.1	47.38 \pm 0.09	39.79 \pm 0.07	65.7 \pm 0.2	64.4 \pm 0.2
09 1322	Sep 9	22h14m05.1s	-0.1	0.03 \pm 0.01	113.2	88.4	48.00 \pm 0.09	39.49 \pm 0.09	66.0 \pm 0.2	64.7 \pm 0.2
09 1323	Sep 9	22h16m00.4s	0.0	0.01 \pm 0.01	101.3	96.1	47.84 \pm 0.09	39.52 \pm 0.08	65.9 \pm 0.2	64.6 \pm 0.2
09 1324	Sep 9	22h16m48.9s	0.5	0.01 \pm 0.01	101.7	97.4	47.66 \pm 0.09	39.89 \pm 0.07	65.8 \pm 0.2	64.6 \pm 0.2
09 1325	Sep 9	22h17m19.4s	-2.1	0.20 \pm 0.08	115.1	99.1	47.86 \pm 0.10	39.41 \pm 0.09	65.9 \pm 0.2	64.6 \pm 0.2
09 1326	Sep 9	22h28m32.1s	-5.1	4.14 \pm 1.68	120.0	95.1	47.73 \pm 0.10	39.78 \pm 0.09	65.8 \pm 0.2	64.5 \pm 0.2
09 1327	Sep 9	22h34m10.6s	-5.8	7.76 \pm 3.14	118.6	93.4	47.95 \pm 0.10	39.65 \pm 0.09	65.8 \pm 0.2	64.6 \pm 0.2
09 1328	Sep 9	22h49m01.2s	-4.9	3.28 \pm 1.33	114.8	92.2	47.61 \pm 0.09	39.45 \pm 0.09	65.9 \pm 0.2	64.7 \pm 0.2
09 1329	Sep 9	22h52m36.7s	-4.8	2.87 \pm 1.16	114.9	90.4	48.05 \pm 0.07	39.34 \pm 0.07	66.0 \pm 0.2	64.8 \pm 0.2
09 1330	Sep 9	23h01m55.9s	1.0	0.01 \pm 0.01	103.6	98.7	47.72 \pm 0.09	39.66 \pm 0.07	65.8 \pm 0.2	64.6 \pm 0.2
09 1331	Sep 9	23h17m15.1s	-5.3	5.23 \pm 2.12	117.8	90.7	47.77 \pm 0.09	39.68 \pm 0.07	65.8 \pm 0.2	64.6 \pm 0.2
09 1332	Sep 9	23h23m59.8s	-4.0	1.42 \pm 0.58	109.7	95.6	47.79 \pm 0.09	39.59 \pm 0.07	65.9 \pm 0.2	64.7 \pm 0.2
09 1333	Sep 9	23h53m01.0s	-3.3	0.64 \pm 0.26	112.6	94.7	48.05 \pm 0.08	39.70 \pm 0.07	66.0 \pm 0.2	64.8 \pm 0.2
101 301	Sep 10	1h46m40.3s	-4.7	2.77 \pm 1.12	109.4	85.8	47.82 \pm 0.12	39.11 \pm 0.09	65.9 \pm 0.2	64.8 \pm 0.2
101 302	Sep 10	2h45m22.9s	1.8	0.01 \pm 0.01	105.2	97.2	47.74 \pm 0.13	39.63 \pm 0.10	65.7 \pm 0.2	64.6 \pm 0.2
101 303	Sep 10	3h16m23.7s	-6.1	11.6 \pm 4.7	120.7	84.4	47.98 \pm 0.15	39.58 \pm 0.12	65.8 \pm 0.2	64.8 \pm 0.2
101 304	Sep 10	4h07m48.6s	-4.1	1.57 \pm 0.64	113.9	92.1	48.09 \pm 0.10	39.74 \pm 0.10	65.6 \pm 0.2	64.6 \pm 0.2
101 305	Sep 10	4h32m30.8s	-6.4	16.1 \pm 6.5	115.9	85.6	47.54 \pm 0.10	39.67 \pm 0.10	65.5 \pm 0.2	64.6 \pm 0.2
101 306	Sep 10	5h16m42.5s	-5.6	6.73 \pm 2.77	113.8	89.6	47.78 \pm 0.10	39.68 \pm 0.10	65.6 \pm 0.2	64.7 \pm 0.2
111 301	Sep 11	3h43m32.7s	-3.9	1.25 \pm 0.50	116.2	95.6	48.12 \pm 0.11	39.75 \pm 0.09	65.4 \pm 0.2	64.4 \pm 0.2
111 302	Sep 11	4h52m52.0s	-5.2	4.73 \pm 1.92	115.8	90.1	49.27 \pm 0.10	39.66 \pm 0.09	65.6 \pm 0.2	64.7 \pm 0.2
111 303	Sep 11	5h06m46.6s	-4.3	0.86 \pm 0.75	114.5	91.7	48.44 \pm 0.12	40.13 \pm 0.10	65.3 \pm 0.2	64.4 \pm 0.2
121 301	Sep 12	0h26m38.1s	-2.0	0.20 \pm 0.08	108.5	97.8	49.37 \pm 0.11	40.77 \pm 0.10	65.6 \pm 0.2	64.4 \pm 0.2
121 302	Sep 12	0h37m57.9s	-4.9	3.50 \pm 1.42	105.7	89.3	49.15 \pm 0.10	40.10 \pm 0.12	65.7 \pm 0.2	64.5 \pm 0.2
121 303	Sep 12	2h11m22.1s	-1.8	0.16 \pm 0.06	105.8	90.6	49.41 \pm 0.10	40.74 \pm 0.10	65.4 \pm 0.2	64.3 \pm 0.2
121 304	Sep 12	23h24m55.5s	-5.9	9.11 \pm 3.69	119.5	90.7	50.00 \pm 0.08	41.10 \pm 0.09	65.4 \pm 0.2	64.2 \pm 0.2

Table 3. Orbital data (J2000) for the SPE meteors listed in Table 2, averaged orbit for $N = 60$ SPE meteors and averaged orbit for meteors recorded during the outburst ($N = 28$).

Meteor code	a (au)	e	i ($^\circ$)	$\Omega \pm 10^{-5}$ ($^\circ$)	ω ($^\circ$)	q (au)	T_j
01 1301	28.4 \pm 14.5	0.972 \pm 0.014	140.29 \pm 0.11	158.717 63	236.1 \pm 0.1	0.789 \pm 0.002	-0.65 \pm 0.37
01 1302	35.9 \pm 23.5	0.978 \pm 0.014	142.71 \pm 0.10	159.385 97	237.0 \pm 0.5	0.781 \pm 0.002	-0.72 \pm 0.47
01 1303	29.9 \pm 16.2	0.974 \pm 0.014	141.55 \pm 0.10	159.487 74	238.1 \pm 0.5	0.774 \pm 0.003	-0.67 \pm 0.39
02 1301	37.3 \pm 25.3	0.979 \pm 0.014	140.59 \pm 0.12	159.563 95	236.6 \pm 0.5	0.784 \pm 0.002	-0.70 \pm 0.47
02 1302	19.2 \pm 6.6	0.959 \pm 0.013	141.13 \pm 0.14	159.623 77	238.2 \pm 0.6	0.775 \pm 0.003	-0.57 \pm 0.27
03 1301	30.2 \pm 16.7	0.975 \pm 0.013	142.20 \pm 0.18	160.538 71	243.4 \pm 0.6	0.733 \pm 0.003	-0.66 \pm 0.39
03 1302	26.6 \pm 13.0	0.971 \pm 0.014	140.55 \pm 0.20	160.638 00	240.4 \pm 0.6	0.757 \pm 0.003	-0.63 \pm 0.35
04 1301	24.8 \pm 11.3	0.970 \pm 0.014	142.70 \pm 0.20	161.493 37	242.7 \pm 0.6	0.739 \pm 0.003	-0.63 \pm 0.34
05 1301	52.7 \pm 51.4	0.985 \pm 0.013	141.75 \pm 0.20	162.470 92	241.3 \pm 0.6	0.747 \pm 0.004	-0.74 \pm 0.65
05 1302	27.3 \pm 13.7	0.973 \pm 0.013	140.42 \pm 0.20	163.274 78	242.9 \pm 0.6	0.737 \pm 0.004	-0.62 \pm 0.36
06 1301	29.9 \pm 16.2	0.975 \pm 0.014	140.69 \pm 0.18	163.590 31	243.5 \pm 0.6	0.732 \pm 0.004	-0.64 \pm 0.38
08 1301	35.9 \pm 23.2	0.980 \pm 0.013	139.53 \pm 0.16	165.424 14	245.6 \pm 0.6	0.714 \pm 0.003	-0.65 \pm 0.43
08 1302	28.2 \pm 14.5	0.974 \pm 0.013	140.89 \pm 0.18	165.469 88	244.2 \pm 0.6	0.726 \pm 0.004	-0.63 \pm 0.36
08 1303	34.3 \pm 21.7	0.979 \pm 0.014	140.73 \pm 0.23	165.491 19	245.4 \pm 0.6	0.716 \pm 0.004	-0.65 \pm 0.43
09 1301	38.3 \pm 26.7	0.981 \pm 0.013	140.24 \pm 0.16	166.309 17	243.7 \pm 0.6	0.729 \pm 0.003	-0.67 \pm 0.47
09 1302	35.4 \pm 22.6	0.980 \pm 0.013	140.09 \pm 0.16	166.335 40	244.1 \pm 0.6	0.726 \pm 0.003	-0.66 \pm 0.43
09 1303	56.6 \pm 58.2	0.987 \pm 0.013	140.27 \pm 0.17	166.361 64	243.9 \pm 0.6	0.726 \pm 0.003	-0.72 \pm 0.66
09 1304	31.5 \pm 17.9	0.977 \pm 0.014	140.04 \pm 0.16	166.365 97	244.4 \pm 0.6	0.724 \pm 0.003	-0.64 \pm 0.39
09 1305	34.6 \pm 21.7	0.978 \pm 0.013	140.49 \pm 0.17	166.403 83	243.7 \pm 0.6	0.730 \pm 0.003	-0.66 \pm 0.43
09 1306	40.4 \pm 29.7	0.982 \pm 0.013	139.74 \pm 0.18	167.179 36	244.7 \pm 0.6	0.721 \pm 0.003	-0.67 \pm 0.48
09 1307	34.6 \pm 21.7	0.979 \pm 0.013	139.30 \pm 0.19	167.185 99	244.5 \pm 0.5	0.723 \pm 0.003	-0.64 \pm 0.43
09 1308	52.3 \pm 48.1	0.986 \pm 0.012	140.00 \pm 0.14	167.188 11	244.6 \pm 0.5	0.721 \pm 0.003	-0.70 \pm 0.60
09 1309	33.8 \pm 20.7	0.978 \pm 0.013	139.06 \pm 0.14	167.188 31	243.7 \pm 0.6	0.728 \pm 0.003	-0.64 \pm 0.41
09 1310	41.5 \pm 31.4	0.982 \pm 0.013	138.92 \pm 0.17	167.189 23	244.0 \pm 0.6	0.726 \pm 0.003	-0.67 \pm 0.49
09 1311	34.3 \pm 21.3	0.980 \pm 0.013	139.10 \pm 0.16	167.190 93	244.8 \pm 0.6	0.721 \pm 0.003	-0.64 \pm 0.41
09 1312	35.7 \pm 23.1	0.979 \pm 0.012	138.95 \pm 0.17	167.191 06	245.1 \pm 0.6	0.718 \pm 0.003	-0.64 \pm 0.43
09 1313	26.7 \pm 12.8	0.973 \pm 0.013	139.13 \pm 0.14	167.191 30	246.0 \pm 0.6	0.712 \pm 0.003	-0.60 \pm 0.33
09 1314	36.7 \pm 24.4	0.980 \pm 0.013	138.71 \pm 0.12	167.192 04	244.5 \pm 0.6	0.722 \pm 0.003	-0.64 \pm 0.44
09 1315	44.7 \pm 36.5	0.983 \pm 0.013	139.00 \pm 0.16	167.193 14	244.4 \pm 0.6	0.723 \pm 0.003	-0.67 \pm 0.52
09 1316	44.9 \pm 36.8	0.983 \pm 0.013	139.21 \pm 0.13	167.193 36	243.6 \pm 0.6	0.729 \pm 0.003	-0.68 \pm 0.54
09 1317	39.9 \pm 29.0	0.981 \pm 0.013	138.88 \pm 0.14	167.193 65	243.8 \pm 0.6	0.728 \pm 0.003	-0.66 \pm 0.48
09 1318	32.4 \pm 19.0	0.977 \pm 0.013	139.41 \pm 0.17	167.193 86	244.5 \pm 0.6	0.723 \pm 0.003	-0.63 \pm 0.40
09 1319	30.5 \pm 16.9	0.976 \pm 0.013	138.56 \pm 0.15	167.195 94	245.0 \pm 0.6	0.720 \pm 0.003	-0.61 \pm 0.37
09 1320	30.4 \pm 16.8	0.976 \pm 0.013	139.45 \pm 0.18	167.197 16	244.4 \pm 0.6	0.724 \pm 0.004	-0.62 \pm 0.38
09 1321	31.1 \pm 17.5	0.977 \pm 0.013	138.53 \pm 0.17	167.199 47	245.0 \pm 0.6	0.720 \pm 0.003	-0.61 \pm 0.38
09 1322	37.6 \pm 25.8	0.981 \pm 0.013	139.56 \pm 0.12	167.199 95	244.0 \pm 0.5	0.726 \pm 0.003	-0.66 \pm 0.45
09 1323	32.2 \pm 18.7	0.978 \pm 0.013	139.36 \pm 0.14	167.201 24	244.4 \pm 0.6	0.724 \pm 0.003	-0.63 \pm 0.39
09 1324	34.4 \pm 21.5	0.979 \pm 0.013	138.63 \pm 0.14	167.201 77	244.1 \pm 0.6	0.726 \pm 0.003	-0.64 \pm 0.42
09 1325	30.0 \pm 16.3	0.976 \pm 0.013	139.54 \pm 0.16	167.202 13	244.6 \pm 0.6	0.722 \pm 0.003	-0.62 \pm 0.37
09 1326	31.4 \pm 17.9	0.977 \pm 0.013	138.80 \pm 0.17	167.209 69	244.2 \pm 0.6	0.725 \pm 0.003	-0.62 \pm 0.39
09 1327	24.9 \pm 11.2	0.971 \pm 0.013	139.19 \pm 0.17	167.213 49	244.3 \pm 0.6	0.726 \pm 0.003	-0.58 \pm 0.32
09 1328	39.9 \pm 29.1	0.982 \pm 0.013	139.29 \pm 0.18	167.223 52	244.9 \pm 0.6	0.719 \pm 0.003	-0.66 \pm 0.48
09 1329	34.1 \pm 21.0	0.979 \pm 0.013	139.81 \pm 0.12	167.225 94	244.3 \pm 0.5	0.725 \pm 0.003	-0.65 \pm 0.42
09 1330	30.4 \pm 16.8	0.976 \pm 0.013	139.00 \pm 0.15	167.232 22	244.6 \pm 0.6	0.723 \pm 0.003	-0.62 \pm 0.38
09 1331	30.1 \pm 16.5	0.976 \pm 0.013	139.01 \pm 0.15	167.242 56	244.5 \pm 0.6	0.724 \pm 0.003	-0.62 \pm 0.37
09 1332	38.2 \pm 26.5	0.981 \pm 0.013	139.21 \pm 0.16	167.247 11	244.4 \pm 0.6	0.723 \pm 0.003	-0.66 \pm 0.46
09 1333	49.8 \pm 44.9	0.985 \pm 0.013	139.24 \pm 0.14	167.266 70	243.5 \pm 0.5	0.730 \pm 0.003	-0.70 \pm 0.58
101 301	45.4 \pm 37.7	0.984 \pm 0.014	139.95 \pm 0.18	167.343 41	245.2 \pm 0.6	0.716 \pm 0.003	-0.68 \pm 0.54
101 302	40.9 \pm 30.6	0.982 \pm 0.014	139.03 \pm 0.20	167.383 01	244.7 \pm 0.6	0.720 \pm 0.004	-0.66 \pm 0.49
101 303	58.1 \pm 62.0	0.987 \pm 0.014	139.25 \pm 0.33	167.403 95	244.2 \pm 0.6	0.724 \pm 0.004	-0.70 \pm 0.67
101 304	34.7 \pm 21.8	0.979 \pm 0.013	139.10 \pm 0.19	167.438 64	244.1 \pm 0.6	0.725 \pm 0.003	-0.64 \pm 0.42
101 305	48.1 \pm 41.0	0.985 \pm 0.013	138.80 \pm 0.20	167.455 31	245.2 \pm 0.6	0.716 \pm 0.004	-0.67 \pm 0.55
101 306	54.6 \pm 54.0	0.986 \pm 0.014	139.00 \pm 0.21	167.455 31	244.6 \pm 0.6	0.721 \pm 0.004	-0.70 \pm 0.62
111 301	38.1 \pm 26.3	0.981 \pm 0.012	138.60 \pm 0.20	168.393 66	246.7 \pm 0.6	0.704 \pm 0.004	-0.64 \pm 0.45
111 302	31.3 \pm 17.7	0.977 \pm 0.013	139.65 \pm 0.19	168.441 17	244.8 \pm 0.6	0.721 \pm 0.003	-0.63 \pm 0.39
111 303	37.1 \pm 25.0	0.981 \pm 0.013	138.23 \pm 0.21	168.450 53	245.6 \pm 0.6	0.714 \pm 0.004	-0.64 \pm 0.44
121 301	48.2 \pm 42.4	0.985 \pm 0.013	137.57 \pm 0.19	169.233 89	244.7 \pm 0.6	0.720 \pm 0.003	-0.66 \pm 0.54
121 302	29.0 \pm 15.1	0.975 \pm 0.012	138.82 \pm 0.18	168.544 58	244.8 \pm 0.6	0.721 \pm 0.003	-0.61 \pm 0.36
121 303	33.5 \pm 20.3	0.978 \pm 0.013	137.56 \pm 0.19	169.304 64	245.1 \pm 0.6	0.718 \pm 0.004	-0.62 \pm 0.40
121 304	35.7 \pm 23.0	0.980 \pm 0.013	137.02 \pm 0.16	170.165 20	245.8 \pm 0.6	0.712 \pm 0.003	-0.62 \pm 0.41
Average ($N = 60$)	36.2 \pm 25.1	0.978 \pm 0.013	139.60 \pm 0.16	166.106 43	243.7 \pm 0.6	0.729 \pm 0.003	-0.65 \pm 0.44
Outburst ($N = 28$)	35.8 \pm 24.0	0.979 \pm 0.013	139.15 \pm 0.16	167.204 62	244.4 \pm 0.6	0.723 \pm 0.003	-0.64 \pm 0.43

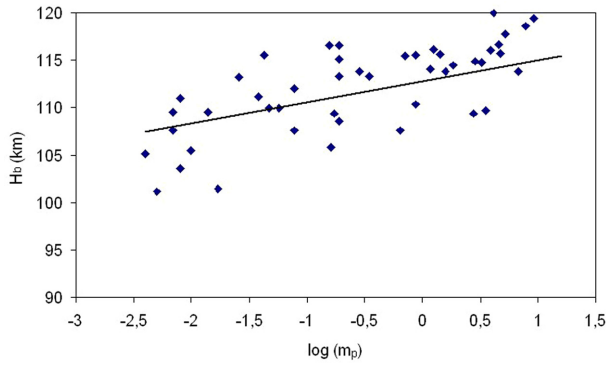


Figure 1. Meteor beginning height H_b versus logarithm of the photometric mass m_p of the meteoroid. Solid line: linear fit for measured data.

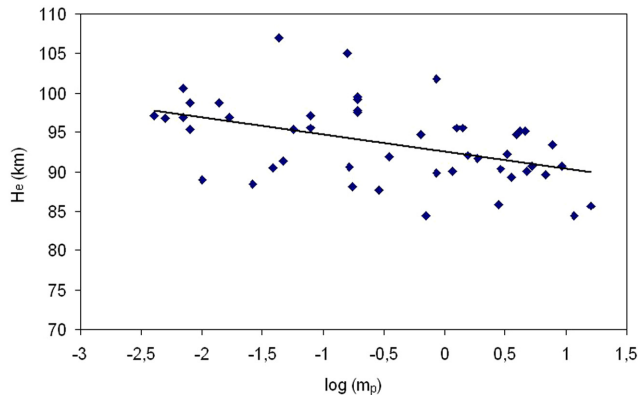


Figure 2. Meteor beginning height H_b versus logarithm of the photometric mass m_p of the meteoroid. Solid line: linear fit for measured data.

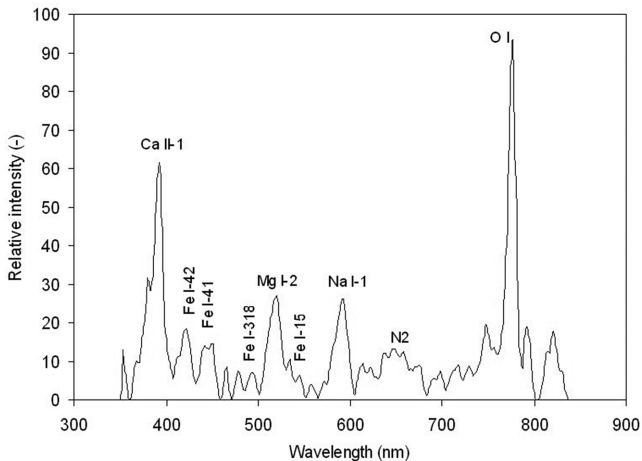


Figure 3. Calibrated emission spectrum of the SPE091327 meteor.

associated with these multiplets was measured frame by frame and subsequently corrected according to the efficiency of the spectrograph. Next, the contributions in each video frame were added to obtain the integrated intensity for each emission line along the meteor path. For the SPE091327 spectrum, the integrated intensities of the Na I-1, Mg I-2, and Fe I-15 multiplets yield 15, 23, and 7, respectively. For the SPE091331 spectrum, these intensities yield 35, 55, and 21, respectively. In this way, we have obtained for the SPE091327 and SPE091331 spectra a Na-to-Mg intensity ratio of

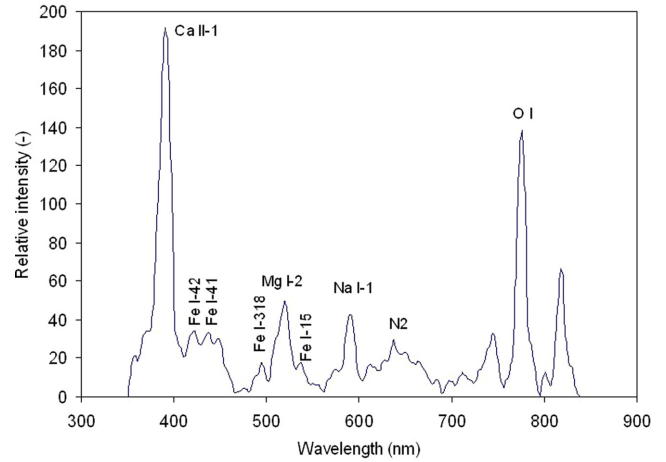


Figure 4. Calibrated emission spectrum of the SPE091331 meteor.

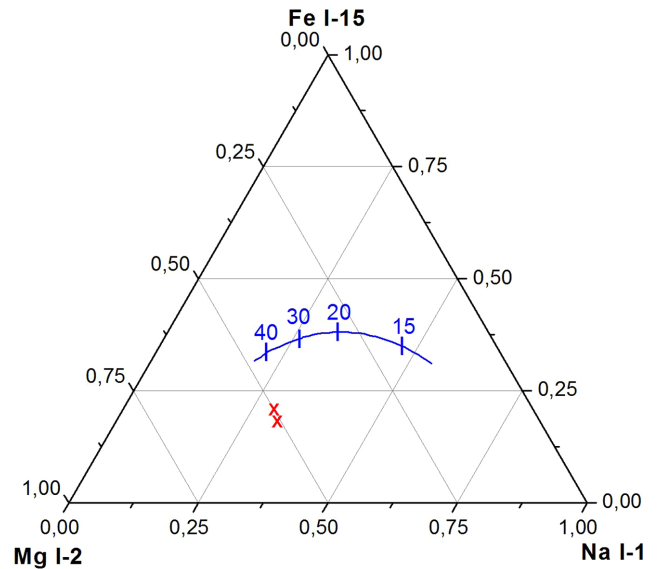


Figure 5. Expected relative intensity (solid line), as a function of meteor velocity (in km s^{-1}), of the Na I-1, Mg I-2, and Fe I-15 multiplets for chondritic meteoroids (Borovička et al. 2005). Crosses: experimental relative intensities obtained for the SPE091327 and SPE091331 spectra.

0.62 and 0.63, respectively. And the Fe/Mg intensity ratio yields 0.29 and 0.38, respectively. The ternary diagram in Fig. 5 shows the relative intensity of the emission from the Na I-1, Mg I-2, and Fe I-15 multiplets for both spectra. The solid curve in this plot corresponds to the expected relative intensity, as a function of meteor velocity, for chondritic meteoroids (Borovička et al. 2005). The position on this solid line corresponding to the velocity of SPE meteors ($\sim 65 \text{ km s}^{-1}$) is not explicitly specified in the work published by Borovička et al. (2005) (see fig. 6 in that work), although the authors of that paper indicate that the points describing these high-speed meteors are located near the left edge of this curve. By taking this into account, we conclude that the points in this diagram describing both spectra show that SPE meteoroids can be considered as normal according to the classification given by Borovička et al. (2005). Thus, the position of these experimental points fits fairly well the expected relative intensity for chondritic meteoroids for a meteor velocity of $\sim 65 \text{ km s}^{-1}$.

5 CONCLUSIONS

We have analysed the meteor activity associated with the SPE meteoroid stream in 2013. In this context, we have observed the outburst experienced by this meteor shower on September 9–10. From the analysis of our recordings, we have reached the following conclusions:

1) The dependence with meteoroid mass of the initial height observed for SPE meteors reveals a cometary origin for this stream. The increase of the beginning height with mass is less important for the SPEs than for the Leonids, the Perseids, the Taurids, and the Orionids. But more pronounced than for the ρ -Geminids and the Geminids. The analysis of the K_B parameter suggests that SPE meteoroids consist of regular cometary material.

2) The orbital data calculated from the analysis of our double-station meteors support the idea that SPE meteoroids are associated with a long-period comet. However, no parent body could be identified among the objects currently included in the Minor Planet Center data base. From this we conclude that the progenitor comet of this meteoroid stream is not yet catalogued.

3) The tensile strength of these meteoroids has been constrained. According to our calculations, the maximum aerodynamic pressure suffered by SPE meteoroids is higher than the tensile strength found for Quadrantid and Perseid meteoroids.

4) We have recorded eight emission spectra produced by SPE meteors during the outburst recorded on September 9–10. Two of these had enough quality to be analysed, and these suggest a chondritic nature for SPE meteoroids.

ACKNOWLEDGEMENTS

We acknowledge support from the Spanish Ministry of Science and Innovation (projects AYA2015–68646-P and AYA 2015–67175-P).

REFERENCES

Borovička J., Koten P., Spurný P., Boček J., Stork R., 2005, *Icarus*, 174, 15
 Bronshten V. A., 1981, *Geophysics and Astrophysics Monographs*. Reidel, Dordrecht
 Ceplecha Z., 1987, *Bull. Astron. Inst. Czech.*, 38, 222

Ceplecha Z., 1988, *Bull. Astron. Inst. Czech.*, 39, 221
 Denning W. F., 1882, *The Obs.*, 5, 262
 Hoffmeister C., 1948, *Die Meteorströme*. Barth, Leipzig
 Jenniskens P., 2004, *AJ*, 127, 3018
 Jenniskens P., 2006, *Meteor Showers and their Parent Comets*. Cambridge Univ. Press, Cambridge
 Jenniskens P., Brower J., Martsching P., Lyytinen E., Entwistle D., Cooke W. J., 2008, *Central Bur. Electron. Telegrams*, 3652, 1
 Jenniskens P., 2013, *Central Bur. Electron. Telegrams*, 3652, 1
 Koten P., Borovička J., Spurný P., Betlem H., Evans S., 2004, *A&A*, 428, 683
 Lindblad B. A., 1971a, *Smithson. Contrib. Astrophys.*, 12, 1
 Lindblad B. A., 1971b, *Smithson. Contrib. Astrophys.*, 12, 14
 Madiedo J. M., Trigo-Rodríguez J. M., 2008, *Earth Moon Planets*, 102, 133
 Madiedo J. M., Trigo-Rodríguez J. M., Ortiz J. L., Morales N., 2010, *Adv. Astron.*, 2010, 167494
 Madiedo J. M., Trigo-Rodríguez J. M., Williams I. P., Ortiz J. L., Cabrera J., 2013a, *MNRAS*, 431, 2464
 Madiedo J. M., Trigo-Rodríguez J. M., Lyytinen E., Dergham J., Pujols P., Ortiz J. L., Cabrera J., 2013b, *MNRAS*, 431, 1678
 Madiedo J. M., Trigo-Rodríguez J. M., Konovalova N., Williams I. P., Castro-Tirado A. J., Ortiz J. L., Cabrera J., 2013c, *MNRAS*, 433, 571
 Madiedo J. M., et al., 2013d, *MNRAS*, 436, 3656
 Madiedo J. M., 2014, *Earth Planet Space*, 66, 70
 Madiedo J. M. et al., 2014, *MNRAS*, 445, 3309
 Madiedo J. M., 2015, *MNRAS*, 448, 2135
 Moore C. E., 1945, *A Multiplet Table of Astrophysical Interest* (Contribution No. 20). Princeton Univ. Observatory, Princeton, NJ
 Picone J. M., Hedin A. E., Drob D. P., Alkin A. C., 2002, *J. Geophys. Res. (Space Phys.)*, 107, 15
 Rendtel J., Molau S., 2010, *WGN, J. IMO*, 38, 161
 Southworth R. B., Hawkins G. S., 1963, *Smithson. Contrib. Astrophys.*, 7, 261
 Trigo-Rodríguez J. M., 1989, *WGN, J. IMO*, 17, 156
 Trigo-Rodríguez J. M., Llorca J., 2006, *MNRAS*, 372, 655
 Trigo-Rodríguez J. M., Llorca J., 2007, *MNRAS*, 375, 415
 Trigo-Rodríguez J. M., Madiedo J. M., Williams I. P., 2009, *MNRAS*, 394, 569
 Williams I. P., 2011, *A&G*, 52, 2.20

This paper has been typeset from a $\text{\TeX}/\text{\LaTeX}$ file prepared by the author.